EXPERIMENTAL STUDIES OF BOUNDARY LAYER DYNAMICS VIA ACTIVE MANIPULATION OF LARGE-SCALE STRUCTURES

Mitchell Lozier
Dept. of Aerospace and Mech. Engineering
University of Notre Dame
Notre Dame, IN, 46556, USA
mlozier@nd.edu

Flint O. Thomas
Dept. of Aerospace and Mech. Engineering
University of Notre Dame
Notre Dame, IN, 46556, USA
fthomas@nd.edu

Stanislav Gordeyev
Dept. of Aerospace and Mech. Engineering
University of Notre Dame
Notre Dame, IN, 46556, USA
sgordeye@nd.edu

ABSTRACT

The dynamic response of a zero pressure gradient turbulent boundary layer (TBL) to a an active flow control actuator was experimentally studied using particle imaging velocimetry (PIV). In previous experiments using a single hot-wire; it was shown that the synthetic large-scale structure (LSS) introduced by this plasma-based actuator in the outer region of TBL had a strong modulating effect on the near-wall turbulence. Results showed that close to the actuator, an actuation frequency comparable to the burst/sweep frequency of the near-wall structure created the strongest modulation effect while farther downstream, an actuation frequency related to the streamwise wavelength of the naturally occurring LSS resulted in the strongest modulation effect. In the study reported here, an improved plasma-based active flow control device was placed in the same region of the TBL to introduce a periodic synthetic LSS in order to study the response of the TBL to these large-scale disturbances. Planar PIV was used to measure the time-resolved two-dimensional velocity downstream of the actuator at a single streamwise location. Using PIV, the modulating effect on the near-wall turbulence is described in more detail. The results are discussed and compared with previous hot-wire measurements and numerical simulations.

INTRODUCTION

It is now widely recognized that vortical large-scale structures (LSS) play a key role in governing the dynamics of wall bounded turbulent flows. The effect of these LSS in turbulent boundary layers (TBL) on technologically relevant flow properties (e.g., friction drag, noise generation, aero-optical distortions, flow separation etc.) have been extensively documented [1-3]. This influence of the LSS on the TBL dynamics was shown to increase with Reynolds number [3]. The dynamics of the LSS have also been shown to be correlated with the near wall small scale turbulence [3,4]. These findings suggest the potential effectiveness of flow control strategies focused on altering the LSS dynamics in to achieve desired technological goals (e.g., reduced drag, noise reduction and separation control). Such strategies could lead to enormous performance gains and cost savings. However, to date, this potential remains largely unrealized due, in large part, to an incomplete understanding regarding the genesis, subsequent evolution and interaction of LSS in the inner and outer regions of the TBL.

In general, the prevailing views fall into two broad groups: (1) those that focus on the influence of outer layer LSS on the near wall turbulence generation mechanism; the so-called" top-down" mechanism and (2) those that view the near wall mechanism as largely autonomous, and the outer LSS results as a consequence of the near-wall turbulence; the "bottom-up" mechanism. Several different models have sought to couple the two regions, with one of the oldest and most notable being the Attached Eddy Model [5], which suggests self-similar eddies with a typical topology of the structure. Mathis et al [4] also modelled these interactions using a correlation-based statistical model where the near-wall effects are predicted from the statistics of the large-scale structures. Both models have proven incredibly useful in understanding the structure of turbulent flows but are limited in that they are statistical in nature and fail to capture the underlying dynamic interaction of the structures. Resolvent analysis is a recent method that overcomes this limitation by looking at spatial-temporal interactions in wall-bounded turbulent flows, thereby providing insight into the dynamics of the structures [6]. Resolvent analysis has proven successful in identifying a key wavenumber-frequency "kernel" or "skeleton" of turbulent pipe flow and answering fundamental questions about the structure of wall-bounded turbulent flows, see e.g. [7].

A vast majority of studies and models regarding the relationship between the near-wall and outer layer large scale structures deal with natural un-manipulated TBLs and apply various conditional averaging techniques are applied to study their interactions [4]. We take the view that to clarify the dynamics of the large-scale structure, one needs to analyse the flow's response to an external large-scale perturbation. Such a dynamic systems approach in which the boundary layer is perturbed via an actuator is particularly well suited to gaining insights regarding the underlying flow physics which is essential for the design of novel active flow control strategies. It artificially introduces a well-defined perturbation with a given frequency and/or spatial scale that allows quantification of the nonlinear TBL response. This approach allows, for instance, the study of triadic interactions between various scales of motion. It also provides a well-defined phase reference by which to perform a phase-locked analysis. In a similar manner, periodic perturbations can also be experimentally introduced into a turbulent boundary layer through a dynamic (temporally oscillating) roughness, which provides a reference phase to
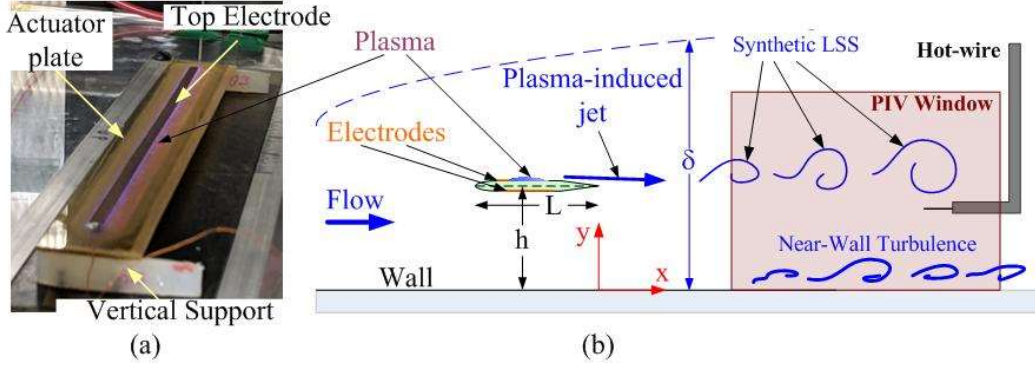
Figure 1. (a) picture of plasma-based ALSSA device and (b) schematic of experimental PIV set-up.

isolate synthetic large-scale structures and small-scale flow structures [8-10]. Instead of introducing the perturbation very close to the wall, Ranade et al. [11] performed an experimental study where the perturbation was introduced in the outer region as a forced shear layer and the turbulence inside the boundary layer was found to be both amplified and modulated by the external forcing. In summary, the introduction of periodic perturbations of the scales of interest has proven an effective way to characterize the flow phenomena of interest.

APPROACH AND EXPERIMENTAL SET-UP

In our previous work [12,13], we introduced large-scale spanwise vorticity into the outer portion of the TBL using a novel active flow control device, called an Active Large-Scale Structure Actuator (ALSSA), see Figure 1(a). The ALSSA was configured to produce a spanwise uniform plasma-induced pulsed jet that serves to introduce coherent spanwise vorticity into the TBL at a specified frequency and wall-normal location. To isolate the interactions of interest, the experimental studies were performed at $Re_\theta = 1770,$, which is low enough that there was no strong naturally occurring large-scale structure in the outer portion of the turbulent boundary layer. This approach allowed the controlled introduction of a synthetic periodic large-scale structure into the TBL. The fixed forcing frequency provides a well-defined reference frequency by which to phase-lock the TBL response and allows clear separation between the large-scale structure and the resulting changes to the TBL dynamics. The advantage of using the plasma-based ALSSA method of actuation is that it introduces the periodic structure at a user-selected location away from the wall without directly affecting the near-wall turbulence.

The experiments were performed in a low-turbulence, subsonic, in-draft wind tunnel located at the University of Notre Dame. To create a canonical turbulent boundary layer, a 2-meter-long by 0.6-meter-wide boundary layer development plate was installed in the centre height of the tunnel test section. Main turbulent boundary layer parameters are summarized in Table 1.

Table 1. Turbulent boundary layer parameters

δ	U	u_τ	C_f	Re_θ	Re_τ
33.2 mm	7.95 m/s	0.304 m/s	0.0039	1,770	690

The rectangular actuator plate was made of a 2 mm thick (0.06δ) sheet of Ultem dielectric polymer. To create plasma, two electrodes were installed on both sides of the actuator plate. The alternating current dielectric barrier discharge (AC-DBD) plasma that formed on top of the actuator was produced using a high voltage AC source. This source provided a 40kV peak-to-peak sinusoidal waveform excitation to the electrodes at a frequency of 4 kHz. The streamwise length of the actuator was chosen to be $L = 32\ mm\ (<\ 1\ \delta)$ to minimize the downstream wake without creating arcing. The spanwise length of the actuator plate was $W = 25\ cm\ (8\ \delta)$ wide. Airfoil-shaped vertical supports were used to position the actuator plate at a fixed wall-normal distance of $h/\delta = 0.3\ (h^+ = 200)$. To introduce periodic forcing, the sinusoidal waveform was modulated by a square wave at the forcing frequency, $f_p = 80\ Hz, (f_p\delta/U_\infty = 0.4)$ with a fifty percent duty cycle.

A schematic of the experimental set-up is shown in Figure 1(b). To quantify the effect of the synthetic large-scale structure on the near-wall turbulence a time-resolved planar PIV system was used. To perform PIV measurements, the flow was seeded with DEHS particles (diameter <1μm) and illuminated with a continuous 532 nm laser sheet ($< 1mm$ spanwise thickness) directed through the top of the test section. The laser sheet was focused onto a small streamwise region ($\Delta x = 6mm, \Delta x/\delta = 0.2$) to produce enough intensity from the continuous laser source to perform PIV. Images were captured with a Phantom v2512 high-speed camera using a $5\mu s$ exposure at a resolution of 384×280 pixel. The measurements presented here were taken at the streamwise locations of $x/\delta = 5$. The frame rate of the camera was 20 kHz (100 U∞/δ), and spatial resolution of the calculated vector fields are $\Delta x^+ = \Delta y^+ = 16$. The PIV acquisition and plasma forcing were triggered simultaneously so that the collected data were phase-locked to the plasma actuation cycle. This PIV configuration resulted in measurements that were time resolved, two-dimensional velocity fields which are also spatial resolved in the wall-normal direction.

RESULTS

Profiles of the streamwise component of mean velocity and turbulence intensity are shown in Figure 2. In Figure 2(a) the canonical mean velocity profile measured using PIV matches the DNS results done with similar turbulent Reynolds number [14]. There is a slight deficit in the mean velocity around the actuator location and extending down towards the wall when the plasma forcing was added. This effect is mostly due to the presence of the actuator plate which creates a wake within the TBL [12]. In Figure 2(b) the canonical turbulence intensity profile is slightly attenuated in the near-wall and log-region due to spatial

averaging caused by the PIV windows. This effect is consistent with the spatial attenuation predicted for hot-wires in [3] as indicated by the ' × ' in Figure 2(b). When the plasma forcing is added there is a deficit in turbulence intensity below the actuator. This reduction in the turbulent intensity in the log-region was found to be mostly due to the presence of the actuator plate [13]. The largest reduction in the turbulence intensity was observed near the location of the actuator, indicated by the dashed line in Figure 2(b). The reduction of the turbulent intensity was observed to extent all the way to the buffer region (y^+~20), as well as in the region above the actuator location. All these results are consistent with the results of the hot-wire experiments documented previously [12,13].
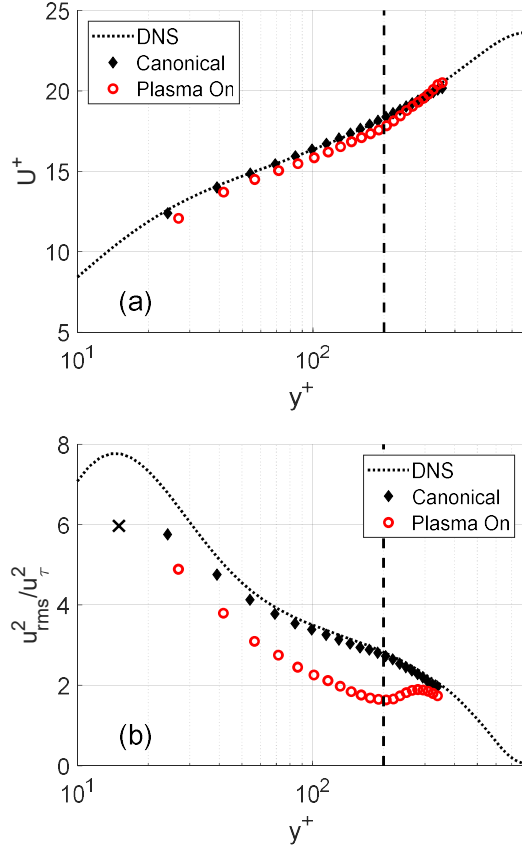

Figure 2. (a) mean streamwise velocity and (b) streamwise turbulence intensity profiles. Vertical dashed line indicates actuator location. Dotted line is DNS data [14]. Black ' × ' represents expected attenuation of turbulence intensity due to spatial averaging. $x = 5\delta, h^+ = 200, f_p = 80Hz$.

In addition to the streamwise velocity components, wall-normal components of velocity have been obtained using PIV. The wall-normal turbulence intensity, Reynolds stress, and turbulence production are presented in Figure 3. In Figure 3(a) the measured canonical turbulence intensity is less than the DNS results due to spatial attenuation in a manner consistent with the streamwise results presented above. When the plasma forcing is added there is a decrease in the turbulence intensity at the actuator location that extends both above and below the actuator. It is expected that for both the streamwise and wall-normal velocity components there will be a reduction in fluctuations due to the presence of the actuator plate with some increase in turbulent fluctuations in the region of the plasma forcing above

the plate described above [12,13]. In Figure 3(b) the measured canonical Reynolds stress ($-\overline{uv}$) is consistently lower than the DNS data throughout the entire boundary layer region due to a combination of the spatial attenuation effects described earlier. When the plasma forcing is added there is a significant decrease in the Reynolds stress around the actuator location that extends both above and below the actuator, like the actuator response for the wall-normal turbulence intensity. In Figure 3(c) the measured canonical turbulence production $\left(-\overline{uv}\frac{\partial \overline{u}}{\partial y}\right)$ matches the DNS results well. When the plasma forcing is added there is a consistent decrease in turbulence production that extends downwards towards the wall. This largest decrease in turbulence in turbulence production occurs around the centre of the log-region and is nearly equal to the canonical production above the actuator location.
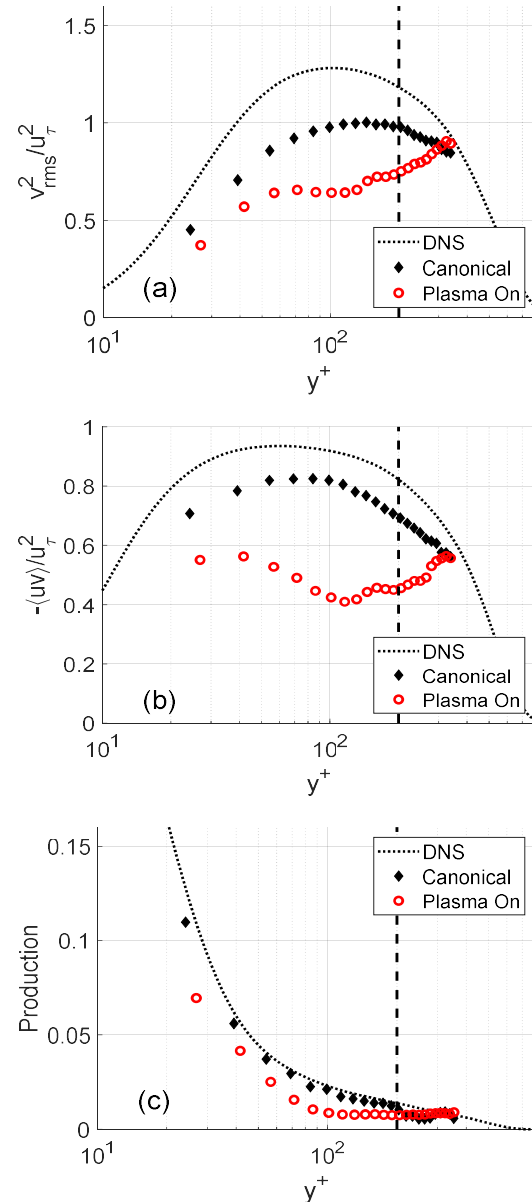

Figure 3. (a) wall-normal turbulence intensity (b) Reynold stress $(-\overline{uv})$ and (c) mean turbulence production $\left(-\overline{uv}\frac{\partial \overline{u}}{\partial y}\right)$ profiles.

Vertical dashed line indicates actuator location. Dotted line is DNS data [14]. $x = 5\delta, h^+ = 200, f_p = 80Hz$.

The mean velocity, turbulence intensity, and Reynolds stress results show different behaviour than those seen in other forced turbulent boundary layers, specifically bottom-up actuation schemes [16]. It was shown that in wall actuated TBL there are generally increases in the turbulence intensity and Reynolds stress in the log and outer regions of the TBL. In this experiment the actuator plate creates a decrease in these quantities while the plasma forcing creates a slight increase above the actuator resulting in an overall decrease in turbulence intensity and Reynold stress.

Because the PIV measurements were phase-locked to the plasma forcing, phase-locked analysis of the PIV measurements was performed using the framework described in [11,12,13], where a triple phase-locked Reynolds decomposition of the streamwise velocity is used,

$$u(x,y,t) = U(x,y) + \tilde{u}(x,y,\varphi) + u'(x,y,\varphi,n).$$

Here u is the instantaneous velocity, U is the time mean component of velocity, $\tilde{u}$ is a phase dependent or modal velocity component, u' is a fluctuating turbulent component, φ is the phase, and n is the number of realizations. To study the fluctuating component, it is convenient to remove the time-averaged term from the phase-locked fluctuating component and investigate the residual phase-changing term only,

$$\Delta u'_{rms}(y,\phi) = u'_{rms}(y,\phi) - \langle u'_{rms}(y,\phi)\rangle_\phi,$$

where,

$$u'_{rms}(x,y,\varphi) = (\langle [u'(x,y,\varphi,n)]^2\rangle_n)^{\frac{1}{2}}$$

The same decomposition was used for the wall-normal, v-component.

The streamwise and wall-normal components of the modal velocity are shown in Figure 4. There are strong modal fluctuations around the actuator location that extend all the way to the near-wall region, as well as to the region above the actuator, for both streamwise and wall-normal components. The strongest variations are around the location of the plasma forcing ($y^+ = 300$ [13,15]) and the geometric centre of the log-region ($y^+ = 100$) where naturally occurring LSS would be present in higher Reynolds number boundary layers. The positive fluctuations in wall-normal modal velocity appear to slightly lead the positive fluctuations in streamwise modal velocity in phase. The modal velocity near the wall lags the velocity in the log-region due to the slower convective speed near the wall. These results are consistent with the hot-wire results presented in [12,13]. In addition, the extracted modal velocity agrees very well with spatial linear input-output analysis [15]. The modal or large-scale response of the TBL to these synthetic outer-layer LSS is very similar to the large-scale response of the TBL to the dynamic roughness observed in [16].
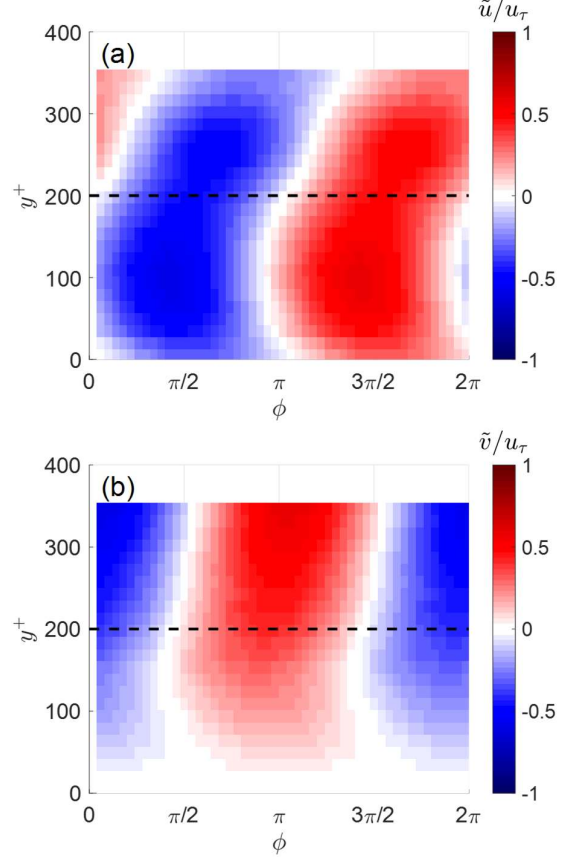

Figure 4. Phase-locked variations in (a) streamwise and (b) wall-normal modal velocity. Actuator location indicated by horizontal dashed line. $x = 5\delta, h^+ = 200, f_p = 80Hz$.

The streamwise and wall-normal components of the residual turbulence are presented in Figure 5. In Figure 5(a) the positive fluctuation in residual turbulence above the actuator location is a signature of the convecting synthetic LSS as described in previous experiments [12,13]. The region of positive fluctuation below the actuator is referred to as the region of modulated near-wall turbulence. This region of modulated turbulence occurs directly below the convecting LSS, and the size, shape and amplitude of the modulated turbulence obtained using PIV is consistent with the results obtained with a hot-wire [12,13]. The region of modulated turbulence extends from the wall through the log-region and has an inclination consistent with canonical near-wall structures [3,13]. The region of modulated streamwise turbulence is slightly leading the positive fluctuations in streamwise modal velocity in phase. This region is also nearly in phase with the wall-normal modal velocity near the wall. In Figure 5(b) there are no significant regions of modulated wall-normal turbulence below the plate, but there are some fluctuations above the plate which are slightly out of phase with the streamwise residual turbulence in a manner consistent with the components of the modal velocity.
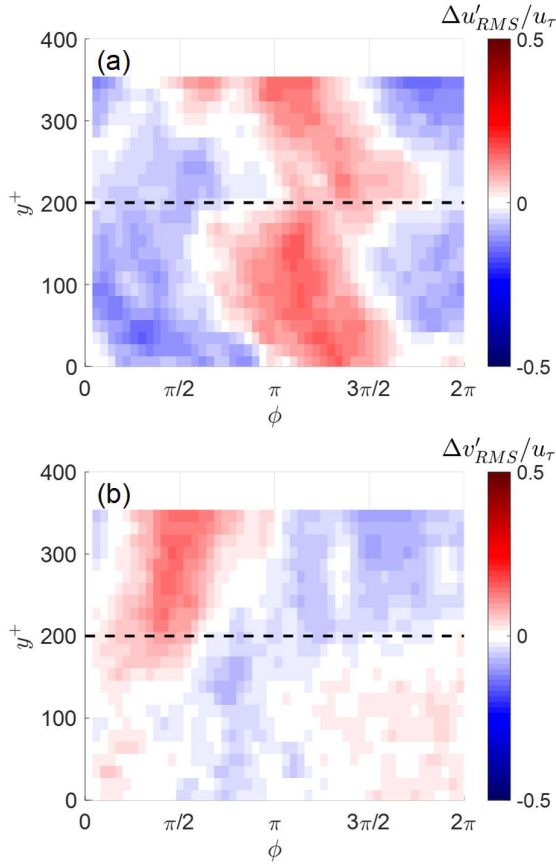
Figure 5. Phase-locked variations in (a) streamwise and (b) wall-normal components of residual turbulence. Actuator location indicated by horizontal dashed line. $x = 5\delta, h^+ = 200, f_p = 80Hz$.
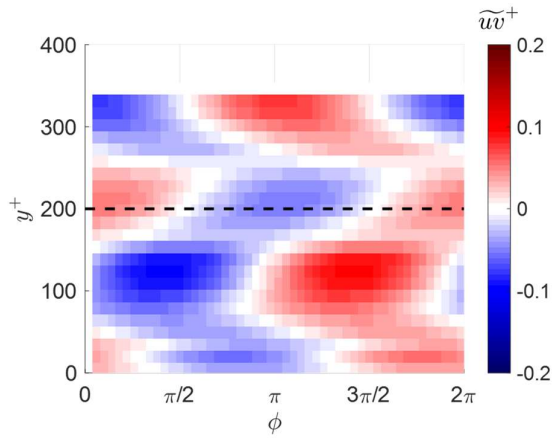

Figure 6. Phase-locked variations in Reynolds stress ($-\widetilde{uv}$) Actuator location indicated by horizontal dashed line. $x = 5\delta, h^+ = 200, f_p = 80Hz$.

The phase-locked decomposition, described above, can also be used to study the modal changes in the Reynolds stress ($-\widetilde{uv}$). The results are shown in Figure 6. There are multiple regions where the modal variations in the Reynolds stress have distinct phases. The strongest variations in Reynolds stress are around the geometric centre of the log-region ($y^+ = 100$) and

the region of the synthetic LSS ($y^+ = 300$). Near the centre of the log-region positive changes in Reynolds stress are approximately in phase with the positive fluctuations in the streamwise modal velocity. These positive Reynolds stress fluctuations also slightly trail the region of modulated turbulence as seen in Figure 5(a). Around the actuator location and near the wall the fluctuations in Reynolds stress are slightly behind the fluctuations at $y^+ = 100$ in phase. This phase delay is likely due to a wall-normal spreading of the Reynolds stress away from the centre of the log-region.

These distinct phase regions highlight the modulating effect of the synthetic LSS. The synthetic LSS cause large-scale velocity fluctuations in the region between the plate and the wall. These fluctuations are correlated with increases in residual turbulence and Reynolds stress. These distinct regions show that the fluctuations in turbulence parameters within the log-region are not induced directly by the LSS but rather are being modulated by LSS presence. The strong changes to turbulence parameters within the log-region, where the natural coherent LSS exist, reinforces previous observations that the forced TBL behaves similarly to a higher Reynolds number canonical boundary layer [12,13] when exciting the scales close to the naturally occurring LSS.
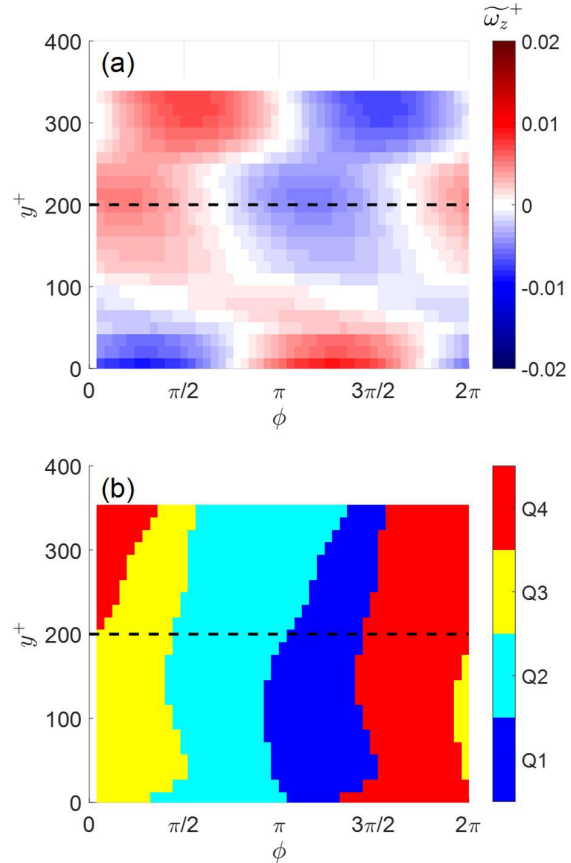

Figure 7. Phase-locked variations in (a) spanwise vorticity and (b) fluctuating velocity quadrants. Actuator location indicated by horizontal dashed line. $x = 5\delta, h^+ = 200, f_p = 80Hz$.

Finally, the phase-locked variations in spanwise vorticity and fluctuating velocity quadrant analysis are presented in Figure 7. From Figure 7(a) the vortical signature of the LSS above the actuator plate can be seen as well as the induced vorticity in the near-wall and log-region. The fluctuations in

spanwise vorticity match the phase of the Reynolds stress and turbulence production fluctuations. It should be kept in mind that later phase corresponds to the earlier spatial location, if a frozen flow assumption is used,

$$x = x_{meas} - \frac{\varphi}{2\pi} \frac{1}{f_p} U_c.$$

Here x is the streamwise pseudo-spatial coordinate, x_{meas} is the measurement location, and U_c is an appropriate convective velocity for the actuator location, see [12] for details. Thus, from Figure 7(b) the quadrant analysis shows that the fluctuations in the velocity in *physical space* follow the $Q4 \rightarrow Q1 \rightarrow Q2 \rightarrow Q3$ pattern. This sequence corresponds to the dynamics of the large-scale structures observed in canonical turbulent boundary layers and plays the most important role in the dynamics and transport of near-wall turbulence [17]. Both the vorticity and quadrant analysis results are consistent with the results of the spatial input-output analysis [15]. It does demonstrate that the synthetic LSS introduced by the plasma actuator has a very similar dynamic effect on the turbulent boundary layer as the naturally-occurring LSS in the higher Reynold number boundary layers.

CONCLUSIONS

PIV measurements of the top-down plasma actuated TBL were made at a single streamwise location and compared to previous experimental works [12,13,16] and numerical simulations [14,15]. In terms of statistical quantities, the plasma-based top-down actuation method resulted in an opposite effect to bottom-up wall actuated methods [16] where all the two-dimensional Reynolds stresses decreased in the log and outer regions instead of increasing due to the presence of an actuator plate. Phase-locked analysis of the modal velocity and residual turbulence showed good agreement with previous work [12,13] as well as numerical simulations [15]. Additionally, analysis of the variations phase-locked variations in Reynolds stress showed that the LSS have a predominantly modulating effect within the log-region and on the near-wall turbulence. Specifically, the LSS create variations localized within the log-region which drive the modulation of the near-wall turbulence. These observations along with the canonical patterns from the quadrant analysis show that the TBL is responding to the presence of LSS in manner consistent with higher Reynolds number canonical boundary layers. These results are consistent with the spectral decomposition of skewness measurements presented in Midya et al [18] which show significant differences between the canonical and actuated TBLs in the logarithmic region.

REFERENCES

[1] Robinson, S.K. (1991) Coherent motions in turbulent boundary layers. Annual Rev. Fluid Mech. 23, 601–639.

[2] M Guala, SE Hommema, RJ Adrian, 2006, "Large-scale and very-large-scale motions in turbulent pipe flow," J. Fluid Mech., 554, pp. 521-542.

[3] N. Hutchins and I. Marusic, 2007, "Large-scale influences in near-wall turbulence," Phil. Trans. R. Soc. A, 365, pp. 647–664.

[4] R. Mathis, N. Hutchins, and I. Marusic, 2011, "A predictive inner–outer model for streamwise turbulence statistics in wall-bounded flows," J. Fluid Mech., 681, pp. 537–566.

[5] de Silva, C. M., Hutchins, N. & Marusic, I., 2016,"Uniform momentum zones in turbulent boundary layers," J. Fluid Mech., 786, pp. 309-331.

[6] McKeon, B. J. and Sharma, A. 2010 "A critical layer framework for turbulent pipe flow," J. Fluid Mech., 659, pp. 336-382.

[7] Sharma, A.S., and McKeon, B.J., 2013. On coherent structure in wall turbulence J. Fluid Mech. 728 pp. 196–238.

[8] Jacobi, I., and McKeon, B. J., 2011, "Dynamic roughness perturbation of a turbulent boundary layer," J. Fluid Mech., 688, pp. 258–296.

[9] Jacobi, I., and McKeon, B. J., 2013, "Phase relationships between large and small scales in the turbulent boundary layer," Exp. Fluids, 54(3), p. 1481.

[10] McKeon, B. J., Jacobi, I., and Duvvuri, S., 2018, "Dynamic roughness for manipulation and control of turbulent boundary layers: an overview," AIAA J., 56(6), pp. 2178–2193.

[11] Ranade, P., Duvvuri, S., McKeon, B., Gordeyev, S., Christensen, K., and Jumper. E.J., 2019," Turbulence Amplitude Amplification in an Externally Forced, Subsonic Turbulent Boundary Layer," AIAA J., 57(9), 3838-3850

[12] Lozier, M.E., Thomas, F.O., and Gordeyev, S., 2020," Streamwise Evolution of Turbulent Boundary Layer Response to Active Control Actuator," AIAA Paper 2020-0097.

[13] Lozier, M.E., Thomas, F.O., and Gordeyev, S., 2021," Turbulent Boundary Layer Response to Active Control Plasma Actuator", AIAA Paper 2021-1455.

[14] Jiminez, J., et. al. 2010, "Turbulent Boundary layers and channels at moderate Reynolds number," JFM 657, 335-360.

[15] Liu, C., et. al. 2022* "Spatial input-output analysis of large-scale structures in actuated turbulent boundary layers," AIAA J.

[16] Huynh, D., McKeon, B., 2020, "Characterization of the Spatio-Temporal Response of a Turbulent Boundary Layer to Dynamic Roughness," Flow, Turbulence and Combustion 104, 293-311.

[17] Nagano, Y., and Tagawa, M., 1995, "Coherent motions and heat transfer in a wall turbulent shear flow," J. Fluid Mech., Vol. 305, pp. 127–157.

[18] Midya, S., Thomas, F. O. and Gordeyev, S. V., "On the Spectral Decomposition of Skewness in Canonical and Actuated Turbulent Boundary Layers," Proceedings of the 12th International Symposium on Turbulence and Shear Flow Phenomena (TSFP12), Osaka, Japan, 2022.